Acta Crystallographica Section B
Structural Science
ISSN 0108-7681

Form, function and functionality of two dimeric toluene-2,4-diisocyanate polymorphs

Liana Vella-Zarb and Robert E. Dinnebier*

Max Planck Institute for Solid State Research, Heisenbergstrasse 1, D-70569 Stuttgart, Germany

Correspondence e-mail: r.dinnebier@fkf.mpg.de

Received 25 January 2012
Accepted 26 February 2012

2,4-Dioxo-1,3-diazetidine-1,3-bis(methyl-*m*-phenylene) diisocyanate (dimerized toluene-2,4-diisocyanate, TDI) is one of the most widely used aromatic diisocyanates in the polymer industry, and it crystallizes in at least two polymorphic forms (form *A* and form *B*) depending on reaction conditions. The crystal structures of the two forms were determined from high-resolution laboratory X-ray powder diffraction data using simulated annealing and Rietveld refinement. In spite of a marked structural similarity between them, significant discrepancies in the physical properties of the two forms prompted analysis of their partitioned energy terms in an effort to better our understanding of the driving force behind such differences in behaviour.

1. Introduction

Polymorphism in molecular crystals is a phenomenon that continues to attract the attention of researchers across many scientific disciplines (Bernstein, 2002), primarily due to the fact that a compound can exhibit significantly different physicochemical properties when its molecules adopt a different arrangement in three-dimensional space. The correlation between crystal structures and their physical properties may go well beyond intermolecular interactions, and insight into the energy landscapes of the different forms may provide a better understanding of the behaviour of such materials.

Toluene diisocyanate is one of the most widely used aromatic diisocyanates, produced as an intermediate in the plastics industry to react with polyols for the formation of polyurethanes. Its primary applications are in the manufacture of adhesives, sprays, foam cushioning for upholstery, elastomers, insulation materials and coatings, with particular use in the formation of high-quality laquers for the car and aviation industries (National Toxicology Program, 2011).

Toluene diisocyanate exists as two isomers, namely toluene-2,4-diisocyanate which is an asymmetrical molecule having two isocyanate groups of very different reactivity, and toluene-2,6-diisocyanate, a symmetrical molecule whose isocyanate groups are equally reactive (Randall & Lee, 2002). Toluene-2,4-diisocyanate is a colourless to pale yellow liquid with a pungent odour, turning pale yellow on exposure to air. Upon dimerization it forms a white powder which crystallizes in at least two polymorphic forms (form *A* and form *B*) depending on reaction conditions.

In spite of a marked similarity between the two forms, significant differences in their physical properties exist. Form *A* is the more flexible material, but it has been found to convert readily to form *B* under ambient conditions.

Table 1
Experimental details.

For all structures: $C_{18}H_{12}N_4O_4$, M_r = 348, $P\bar{1}$. Experiments were carried out at 298 K with Cu $K\alpha$ radiation, λ = 1.54059 Å.

Polymorph	Form *A*	Form *B*
Crystal data		
a, *b*, *c* (Å)	4.53125 (8), 5.99235 (8), 14.7567 (3)	9.09477 (8), 7.45366 (5), 12.75989 (16)
α, β, γ (°)	88.2562 (12), 81.6029 (15), 81.2337 (13)	93.5753 (8), 99.7115 (6), 114.0050 (6)
V (Å^3)	391.75 (1)	770.56 (1)
Z	1	2
ρ (calc) (g cm^{-3})	1.477	1.501
Data collection		
Diffractometer	Bruker D8 ADVANCE	Bruker D8 ADVANCE
Specimen mounting	Capillary	Capillary
Data collection mode	Transmission	Transmission
Scan method	Step	Step
2θ values (°)	$2\theta_{min}$ = 5.0, $2\theta_{max}$ = 68.3, $2\theta_{step}$ = 0.009	$2\theta_{min}$ = 5.0, $2\theta_{max}$ = 67.4, $2\theta_{step}$ = 0.009
Refinement		
R factors and goodness-of-fit	R_p = 0.036, R_{wp} = 0.050, R_{exp} = 0.015, R_{Bragg} = 0.026, χ^2 = 3.39	R_p = 0.019, R_{wp} = 0.025, R_{exp} = 0.012, R_{Bragg} = 0.006, χ^2 = 2.08
No. of datapoints	7362	7268
No. of parameters	63	150
No. of restraints	47	104

In this paper we report the crystal structures of the two TDI dimer polymorphs solved from high-resolution laboratory X-ray powder diffraction data, together with an examination of their packing features by comparison of their total lattice energies and the respective coulombic, polarization, dispersion and repulsion contributions.

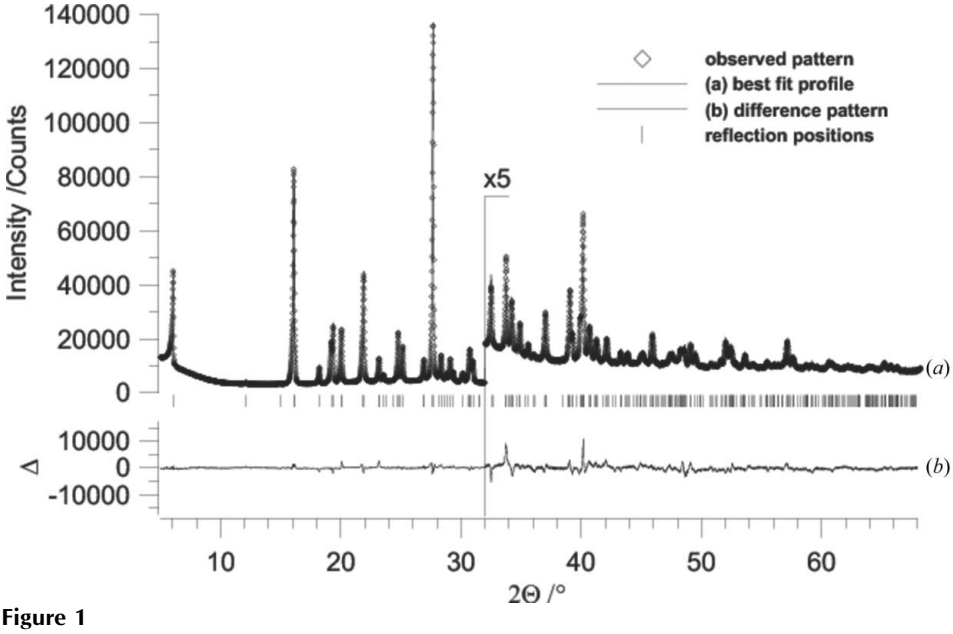

Figure 1
Scattered X-ray intensity for dimeric TDIC form *A* as a function of diffraction angle 2θ. The observed pattern (diamonds), the best Rietveld-fit profile (*a*), the difference curve between observed and calculated profile (*b*), and the reflection markers (vertical bars) are shown. The wavelength was λ = 1.5406 Å. The higher-angle part of the plot starting at 32° 2θ is enlarged for clarity.

2. Experimental

2.1. Sample preparation

A sample of each polymorph of dimerized toluene-2,4-diisocyanate was received from Rhein Chemie Rheinau GmbH, Düsseldorfer Strasse 23-27, 68219 Mannheim, and used without further purification. A few milligrams of each sample were ground gently in an agate mortar and immediately filled into borosilicate glass capillaries (Hilgenberg Glass No. 50) of diameter 0.7 which were later sealed.

2.2. X-ray powder diffraction

X-ray powder diffraction patterns were recorded at room temperature on a Bruker D8 ADVANCE high-resolution laboratory X-ray powder diffractometer using Cu $K\alpha_1$ radiation from a primary Ge(111)-Johanson-type monochromator and a Våntec position-sensitive detector (PSD) in Debye–Scherrer geometry. Data collection for each sample spanned over 20 h, covering a range of 2–65° along 2θ in steps of 0.008° with a 6° opening of the PSD. To ensure better particle statistics, the samples were spun during measurement.

2.3. Data analysis

For structure determination and refinement, the program *TOPAS*4.1 (Bruker, 2007) was used. The powder diffraction patterns of form *A* and form *B* were indexed with the singular value decomposition method as implemented within *TOPAS* (Coelho, 2003), resulting in primitive triclinic unit cells for both polymorphs (Table 1). Of the only possible space groups *P*1 (1) and $P\bar{1}$ (2), the latter could be confirmed by Rietveld refinements (Rietveld, 1969). From volume increments *Z* was determined to be 1 for form *A* and 2 for form *B*. The peak profile and precise lattice parameters were determined by Le Bail fits (Le Bail *et al.*, 1988) using the fundamental parameter (FP) approach of *TOPAS* (Cheary *et al.*,

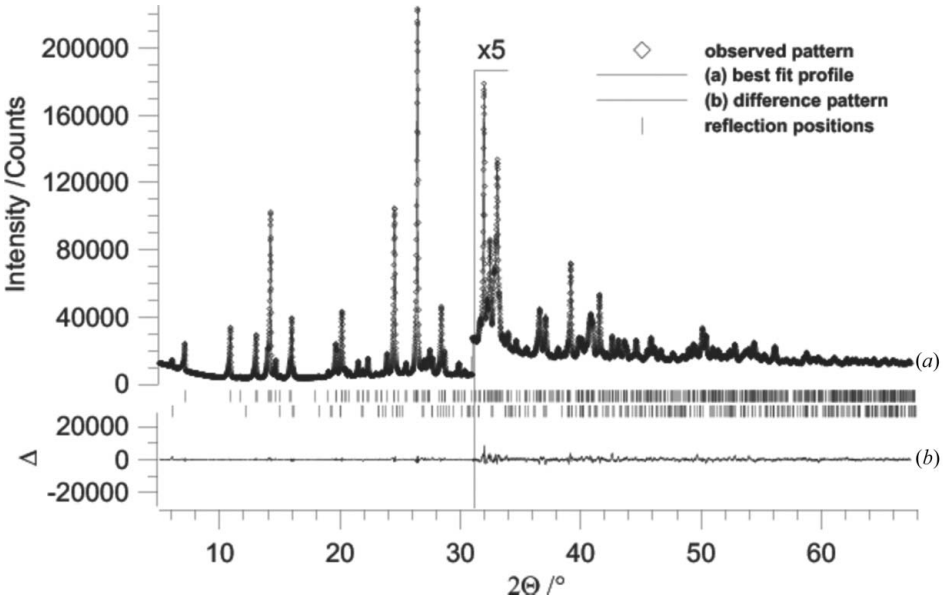

Figure 2
Scattered X-ray intensity for dimeric TDIC form *B* as a function of diffraction angle 2θ. The observed pattern (diamonds), the best Rietveld-fit profile (*a*), the difference curve between observed and calculated profile (*b*), and the reflection markers (vertical bars) are shown. The wavelength was λ = 1.5406 Å. The higher-angle part of the plot starting at 31°2θ is enlarged for clarity. Weight percentage of form *B* (top phase) = 95.9%, and form *A* (bottom phase) = 4.1%.

2007), allowing for the determination of microstructural properties such as domain size and microstrain. For the modelling of the background, fifth-order Chebychev polynomials were employed.

The crystal structures of both polymorphs of dimeric toluene-2,4-diisocyanate were solved by the global optimization method of simulated annealing (SA) in real space as implemented by *TOPAS* (Coelho, 2000). Since the position and connectivity of the cyanate group was not known *a priori*, two independent rigid bodies were set up in the rigid-body editor of *TOPAS* using standard bond lengths and angles. Slack bond-length, bond-angle and planarity restraints were introduced to stabilize the subsequent Rietveld refinement.

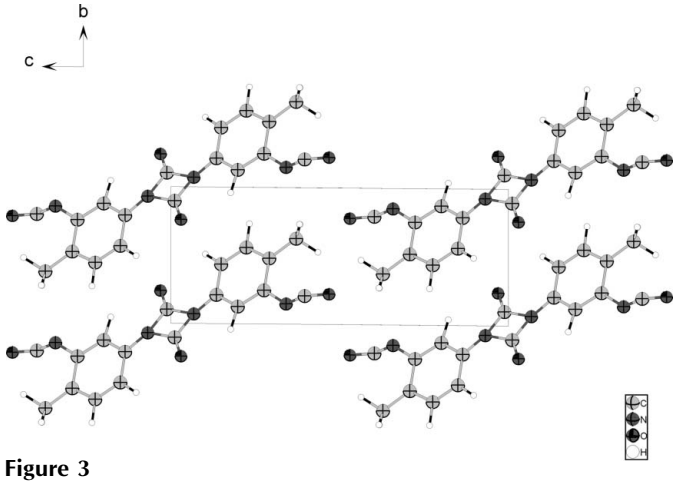

Figure 3
Form *A* viewed along the *a* axis. The probability for non-hydrogen spheroids is 50%, while that of hydrogen spheroids is 20%.

For the final Rietveld refinement, all profile and lattice parameters were released and all atomic positions were subjected to refinement using soft bond and angle constraints (Figs. 1 and 2). While form *A* was found to be pure, the powder pattern obtained for form *B* revealed an admixture of the two phases. The weight percentage of this mixture, determined by quantitative Rietveld refinement, was 95.9% form *B* and 4.1% form *A*. Final agreement factors (*R* values) are listed in Table 1. The full list of atomic coordinates for both forms, together with intramolecular distances and angles, can be found in the supplementary information.[1]

2.4. Lattice-energy calculations

For the purpose of this study, molecules were treated as rigid, and thus intramolecular energies were not considered. Intermolecular energies were calculated using the atom–atom method found within the atom–atom, Coulomb–London–Pauli (AA–CLP) package (Gavezzotti, 2011), which describes molecular structures by coordinates for the location of the atomic nuclei. H atoms were re-assigned and re-calculated at a C—H distance of 1.08 Å, and the calculated interaction energies were categorized as coulombic, polarization, dispersion and repulsion terms. This subdivision of the total lattice energy takes into account the electron distribution and polarization, allowing for a more straightforward structure-based chemical interpretation than would be possible with one total energy value alone (Gavezzotti, 2011).

The AA–CLP package makes use of charge densities and their electric fields for the determination of coulombic and linear-polarization terms, while the London approach (London, 1937) is used to evaluate quantum hyperpolarization (dispersion) terms in view of electron correlation. Pauli spin avoidance (Kauzmann, 1957) takes into account the extent of overlap between neighbouring charge densities in order to establish the degree of repulsion.

3. Results and discussion

3.1. Crystal structures of the two forms of toluene-2,4-diisocyanate dimers

The crystal structures of form *A* and form *B* have been solved and refined from high-resolution laboratory X-ray

[1] Supplementary data for this paper are available from the IUCr electronic archives (Reference: KD5060). Services for accessing these data are described at the back of the journal.

powder diffraction data. Refinements with different amounts of *cis*- and *trans* isomers did not improve agreement factors, and both polymorphs were found to crystallize exclusively in the 2,4-*trans* configuration. Crystallographic details are summarized in Table 1, and the final Rietveld plots are given in Figs. 1 and 2.

The unit-cell volume of form *B* was found to be almost double that of form *A*, possibly due to a difference in molecular packing flexibility. In form *A* the centre of symmetry of the molecule lies directly on the centre of symmetry of the space group $P\overline{1}$, thus posing torsional restrictions. Form *B* does not exhibit such restrictions (Figs. 3 and 4). This is evident from the different torsion angles of the end-standing NCO groups which thus enable optimized crystal packing, also resulting in a slight increase in density. Fig. 5 and Table 2 summarize the main differences in torsion angles between the two polymorphs.

Form *A* and form *B* exhibit a clearly visible difference in their packing schemes. In form *B* the molecules are arranged in infinite parallel stacks parallel to the *c* axis, adopting a ribbon-like formation perpendicular to the *a* direction. Although in form *A* the molecules also show stacking, this is not observed along any of the crystallographic axes, and consecutive molecules within the stacks are shifted by approximately 4 Å perpendicular to the stacking direction (Figs. 6 and 7).

Table 2
Numerical comparison of the differences in torsion angles (°) for form *A* and form *B*, including the torsions necessary for the conversion of one form into the other.

Torsions 1 and 4 show strong interdependence, especially in form *A*. (+) denotes clockwise torsion while (−) denotes anticlockwise torsion.

C═C−N═C	Form *A*	Form *B*	Δ form *A* → form *B*
1	−150.89	+161.05	−48.06
2	+9.53	−1.77	−11.30
3	−36.67	−12.51	+24.16
4	−150.88	+173.27	−33.85

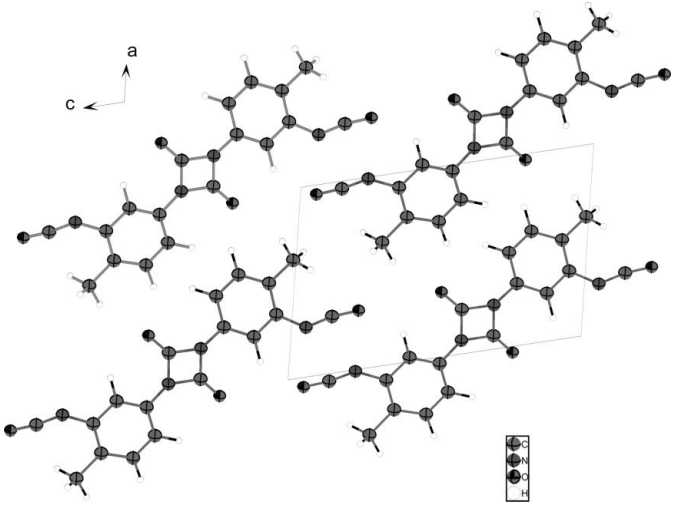

Figure 4
Form *B* viewed along the *b* axis. The probability for non-hydrogen spheroids is 50%, while that of hydrogen spheroids is 20%.

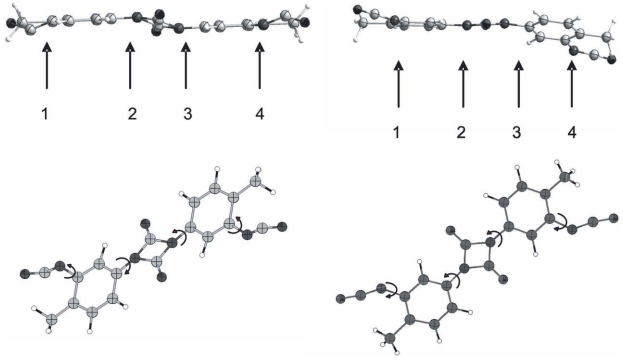

Figure 5
Visual comparison of the differences in torsion angles for form *A* (left) and form *B* (right). Red arrows denote anticlockwise (−) torsion, while blue arrows denote clockwise (+) torsion.

3.2. Lattice-energy calculations

From the lattice-energy calculations obtained *via* the CLP package (Gavezzotti, 2011) it is observed that form *B* is the more stable structure out of the two. This is reflected in its density which is higher than that of form *A*, albeit slightly. The total lattice energies, as well as coulombic, polarization, dispersion and repulsion contributions, are also very close between the two forms. These energy values are summarized in Table 3. Conversion of form *A* to the more stable form *B* requires a translation vector *T* with respect to the crystallographic base of form *A*, where *T* = (0 / 1.2 / 6.5) Å, in addition to the torsion changes listed in Table 2. Although the packing of the two polymorphs is different, the ability to convert one into the other by simple operations accounts for the relatively small difference in their lattice energies. For both forms, the dispersion energy and repulsion terms represent the most significant contributions. In terms of the interaction energies between two closest neighbouring molecules, the differences between the forms are rather small. Dispersion energy terms for both polymorphs lie within the range −1.7 to −73.4 kJ mol^{-1}, and in all cases are lower than the corresponding coulombic terms. The higher repulsion energy in

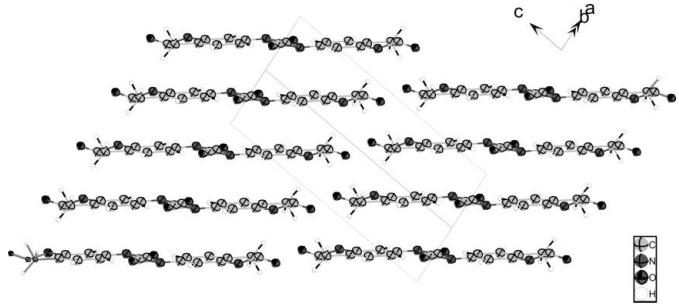

Figure 6
Stacking arrangement in form *A* showing parallel flat sheets.

Table 3
Intermolecular energies (values are given per molecule in the asymmetric unit).

	Intermolecular interaction energy (kJ mol^{-1})				
	Coulombic	Polarization	Dispersion	Repulsion	Total
Form *A*	−18.5	−68.1	−184.0	+84.8	−185.8
Form *B*	−17.5	−68.0	−189.0	+79.3	−195.1

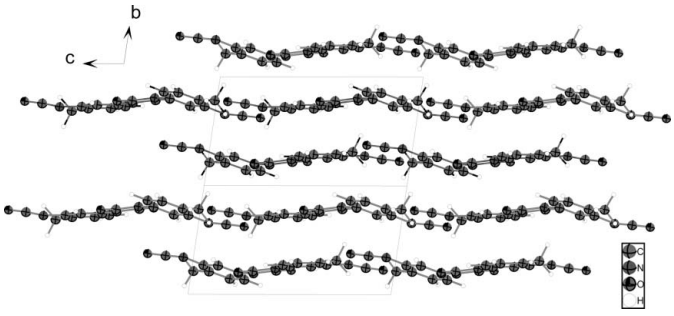

Figure 7
Form *B* forming folded sheets showing a stacking arrangement along the short *b* axis.

form *A* could be due to the fact that the distance between the centres of mass is smaller, thus resulting in a stronger repulsive force. This, coupled with the slight difference in energy of dispersion, contributes to the greater thermodynamic stability of form *B*.

4. Conclusions

The structures of two polymorphs of toluene-2,4-diisocyanate have been successfully solved from laboratory X-ray powder diffraction data. Clear differences between the two thermodynamically similar polymorphs have been observed, and these have been highlighted by analysis and comparison of the partitioned energy terms. Dispersion and repulsion contributions play a very important role in the total energy landscape of these forms. Calculated lattice energies suggest that form *B* is slightly more thermodynamically stable than form *A*, providing an energetic justification for the preferential conversion of one form into the other. Although they exhibit different packing arrangements, both forms of dimeric TDIC feature stacks and in form *B* these are observed along a short crystallographic axis. In such cases the stacking interactions gave a stronger stabilizing effect, further accounting for the lower lattice energy of form *B*. In addition, the fact that form *B* has no centre of molecular symmetry located on a crystallographic centre of symmetry allows a more flexible arrangement of the molecules within the structure, resulting in a denser packing scheme. The less dense packing of form *A* accounts for the better flexibility of the material when compared with form *B*, in spite of the latter exhibiting better molecular flexibility on closer scrutiny.

References

Bernstein, J. (2002). *Polymorphism in Molecular Crystals.* Oxford University Press.
Bruker (2007). *TOPAS*, Version 4.1. Bruker AXS, Madison, Wisconsin, USA.
Cheary, R. W., Coelho, A. A. & Cline, J. P. (2007). *J. Res. Natl Inst. Stand. Technol.* **109**, 1–25.
Coelho, A. A. (2000). *J. Appl. Cryst.* **33**, 899–908.
Coelho, A. A. (2003). *J. Appl. Cryst.* **36**, 86–95.
Gavezzotti, A. (2011). *New J. Chem.* **35**, 1360–1368.
Kauzmann, W. (1957). *Quantum Chemistry, An Introduction.* New York: Academic Press.
Le Bail, A., Duroy, H. & Fourquet, J. L. (1988). *Mater. Res. Bull.* **23**, 447–452.
London, F. (1937). *Trans. Faraday Soc.* **33**, 8–26.
National Toxicology Program (2011). Report on Carcinogens, 12th ed. Research Triangle Park, NC: US Department of Health and Human Services, Public Health Service, National Toxicology Program.
Randall, D. & Lee, S. (2002). *The Polyurethanes Book*. New York: Wiley.
Rietveld, H. M. (1969). *J. Appl. Cryst.* **2**, 65–71.